ACS APPLIED MATERIALS & INTERFACES

Research Article

www.acsami.org

Temperature Dependent Photoluminescence of Size-Purified Silicon Nanocrystals

Austin R. Van Sickle,[†] Joseph B. Miller,[†] Christopher Moore,[†] Rebecca J. Anthony,[‡] Uwe R. Kortshagen,[‡] and Erik K. Hobbie*[,†]

[†]Department of Physics and Department of Coatings and Polymeric Materials, North Dakota State University, Fargo, North Dakota 58108, United States

[‡]Department of Mechanical Engineering, University of Minnesota, Minneapolis, Minnesota 55455, United States

Supporting Information

ABSTRACT: The photoluminescence (PL) of size-purified silicon nanocrystals is measured as a function of temperature and nanoparticle size for pure nanocrystal films and polydimethylsiloxane (PDMS) nanocomposites. The temperature dependence of the bandgap is the same for both sample types, being measurably different from that of bulk silicon because of quantum confinement. Our results also suggest weaker interparticle and environmental coupling in the nanocomposites, with enhanced PL and an unexpected dependence of lifetime on size for the pure nanocrystal films at low temperatures. We interpret these results through differences in the low-temperature size dependence of the ensemble nonradiative equilibrium constants. The response of the PDMS nanocomposites provides a consistent measure of local temperature through intensity, lifetime, and wavelength in a polymer-dispersed morphology suitable for biomedical applications, and we exploit this to fabricate a small-footprint fiber-optic cryothermometer. A comparison of the two sample types offers fundamental insight into the photoluminescent behavior of silicon nanocrystal ensembles.

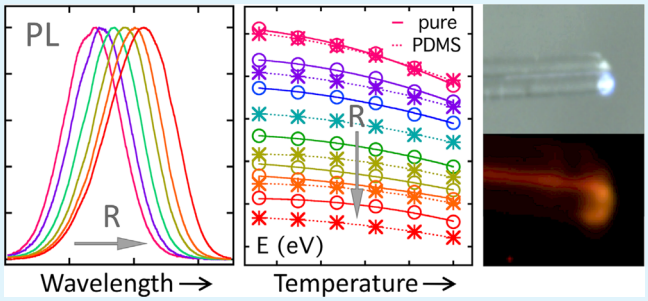

KEYWORDS: *nanocrystalline silicon, polymer nanocomposites, photoluminescence*

INTRODUCTION

The unique optical and electronic properties of semiconductor nanocrystals have generated a tremendous amount of interest directed at a broad range of potential applications.[1−8] Although most of the focus has been on nanocrystals synthesized in solution from precursors of binary alloys such as cadmium selenide, an increasing amount of attention is being directed at silicon, an abundant and technologically well-established element that can be synthesized into nanocrystals of controlled mean size through a single-step process in a low-pressure nonthermal plasma.[9,10] Silicon nanocrystals (SiNCs) produced in this manner have a bright photoluminescence (PL) with a relatively high quantum yield that can be tuned across the visible spectrum to the near-infrared (NIR).[11] In general, SiNCs have low toxicity,[12] good solubility,[13] and high colloidal and intracellular mobility,[14] which makes them excellent candidates for a number of potential applications, ranging from imaging contrast agents[15] to luminescent inks[16] and electron-acceptor materials in photovoltaic devices.[17] In particular, efficient emission in the NIR,[18] a spectral regime where biological tissues are relatively transparent,[19] coupled with good biocompatibility[20] make SiNCs ideal candidates for applications that seek to exploit nanocrystal PL within tissues or biological fluids.

Like all semiconductor nanocrystals, the PL from SiNCs is intimately shaped by quantum confinement.[21] In addition to a strong dependence of emission color on particle size, overlap in the electron−hole pair leads to faster recombination and a reduction in the rate of nonradiative events that typify the bulk material.[22] The indirect nature of the bandgap, however, significantly broadens the emission and leads to lifetimes on the order of 10−100 μs, which stands in stark contrast to the behavior of direct bandgap materials. An area of application where this difference might be beneficial is thermometry based on the PL from quantum dots.[23−30] As one example, cryosurgery at liquid nitrogen temperatures is emerging as a particularly effective way to treat certain internal cancers,[31] but to fully destroy the tumor it is critical to achieve a uniformly low temperature throughout the target.[32] Currently employed metrics for monitoring temperature during cryosurgery are based on ultrasound or magnetic resonance imaging, which provide good spatial resolution but lack thermal sensitivity. Most work to date has focused on CdSe, which exhibits a 5-fold increase in PL between 300 and 100 K.[23] The potential

Received: January 30, 2013
Accepted: April 29, 2013
Published: April 29, 2013

cytotoxicity of CdSe might be unacceptable for biomedical applications,[7,8] however, and SiNCs thus represent a more attractive option for the fabrication such devices.

There has been a small but significant amount of recent work on the temperature dependent PL from SiNCs dispersed in a variety of environments.[33−37] In general, the intensity and lifetime both increase with decreasing temperature as the influence of nonradiative effects decreases, while the emission peak shifts because of thermal changes in the bandgap.[33−37] Only a coarse picture of how the response varies with nanocrystal size has emerged, however, and this has focused primarily on the influence of quantum confinement.[33,37] The potential importance of many-body effects in SiNC ensembles is emerging as a topic of interest, and recent results suggest that nanocrystal size and polydispersity can play a role in the collective optical response.[38,39] In this regard, a temperature dependent PL study has never been performed on size-purified plasma-synthesized SiNCs, and from the perspective of applications that seek to encapsulate the nanocrystals in a protective matrix, the influence of a surrounding polymer on the cryogenic behavior of SiNCs has never been investigated. Such questions are highly relevant to the development of cryogenic sensing applications that exploit the PL from SiNCs, but they also offer more general insight into the fundamental nature of PL from semiconductor nanocrystal ensembles.

Here, we report on the temperature dependent PL of size-purified SiNCs in both pure nanocrystal films and polydimethylsiloxane (PDMS) nanocomposites, and we exploit the results to fabricate the first PL-based SiNC cryoprobe. As might be anticipated, each scenario (pure nanocrystal vs. polymer nanocomposite) shows an appreciable increase in PL intensity and lifetime with decreasing temperature, while the size-dependent bandgap exhibits a common temperature dependence that is measurably different from the thermal behavior of bulk silicon. In addition, however, our measurements reveal an unanticipated increase in lifetime with decreasing nanocrystal size at low-temperature in the pure SiNC films, which as a consequence can exhibit greater fluorothermal sensitivity. We interpret this result through the size dependence of an effective nonradiative equilibrium constant for the low-temperature ensemble, and we compare it with theoretical predictions. Significant insight into the origin of the trend comes from its absence in the polymer nanocomposites, which our results suggest are nonetheless superior materials for fabricating small-footprint fiber-optic cryothermometers. In a much broader view, our results have relevance to any application that seeks to exploit the PL of SiNC ensembles or SiNCs embedded in a polymer matrix, including LEDs, photo and thermo responsive polymer nanocomposites, and SiNC-aggregate fluorophores for bioimaging applications.

RESULTS AND DISCUSSION

The materials are plasma-synthesized SiNCs covalently capped with 1-dodecene, where the ligand imparts solubility in common organic solvents. Details of the plasma synthesis scheme are given elsewhere.[9,10,40] The mean nanocrystal size in the parent is 4 nm with a standard deviation of 0.8 nm (polydispersity index of 1.05), and the microstructure is in excellent agreement with the diamond structure of silicon.[39] Size purification was achieved through density-gradient ultracentrifugation (DGU) in organic solvents as described elsewhere.[39] Two separate sets of comparable fractions from the same parent material were used to make the pure SiNC films and nanocomposites, respectively. Increasing fraction number corresponds to greater depth in the density gradient and hence larger nanocrystal size, where typical fractions have a polydispersity index of 1.01 (standard deviation of 0.35 nm, Supporting Information). The absolute quantum yield of the parent is near 30% immediately after synthesis and processing, while that of the fractions is comparable to the parent for the larger fractions but decreases dramatically with size for the smaller fractions (Supporting Information).[39] As a polymer matrix, we use cross-linked PDMS because of its widely established biocompatibility and biodurability, and we focus on the temperature range relevant to cryomedical applications that employ liquid nitrogen (80 to 300 K). Differential scanning calorimetry (DSC) measurements of the pure PDMS show a single glass transition at $T_g \approx -125$ °C, and there is a small decrease in the optical transmission of the pure PDMS from ambient down to T_g (Supporting Information). Further details are given in the Materials and Methods section.

Figure 1 shows the PL spectrum of the parent at 80 K, PL spectra of the fractions as pure films and PDMS nanocomposites at 80 K, and typical changes in PL with temperature. Use of the fractions over the parent (AP) material offers a clear and significant reduction in PL line width, which will be important for spectral and imaging applications. The difference in PL behavior demonstrated in Figure 1c arises primarily from a difference in the temperature dependence of the quantum yield between the pure SiNC and PDMS nanocomposite samples, but there is also a slight decrease in the optical transmission of PDMS below T_g (Supporting Information). Fraction linewidths are among the lowest reported for nanocrystalline silicon; roughly 1.4× that of commercially available CdSe at comparable emission energy. Figure 2a shows how E, the energy of peak PL, evolves with T, where the excitation power was maintained below 50 mW/cm^2 to avoid low-T saturation effects associated with PL lifetime.[33] In all cases, the PL intensity increased monotonically with decreasing temperature for excitation powers down to 0.2 mW/cm^2. The PL peak shifts to lower energy with increasing T because of thermally induced changes in the quantum-confined energy levels, where such changes can depend on lattice spacing, strain, and electron−phonon coupling.[34,41]

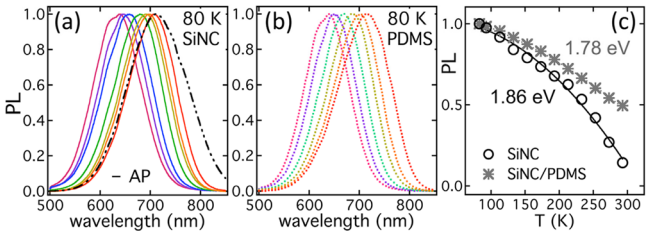

Figure 1. (a) Low-temperature (80 K) PL spectra of pure SiNC films from the fractions, where the black curve is the emission spectrum of the as-produced (AP) material at 80 K. (b) Low-temperature (80 K) spectra of SiNC/PDMS nanocomposites made from comparable fractions. (c) Temperature dependent PL for a pure SiNC fraction (1.86 eV peak emission) and a fraction in PDMS (1.78 eV peak emission), both normalized by the emission at 80 K.

Thermal changes in the bulk Si bandgap occur predominantly through thermal expansion and electron−phonon interactions.[34,42] For quantum dots in general,[41] thermal expansion can affect $E(T)$ through its dependence on lattice spacing a, with $(\partial E/\partial T)_a = (\partial E/\partial a)\ (\partial a/\partial T)$. Such a

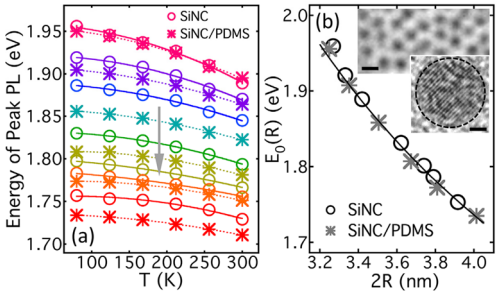

Figure 2. (a) Temperature dependence of the energy of peak PL for both pure SiNC fractions and PDMS nanocomposites, where the arrow indicates the direction of increasing size. (b) Size dependence of the fitting parameter representing the 0 K bandgap, where the upper insets show TEM images of a typical fraction (top, 5 nm scale) and a single nanocrystal (bottom, 1 nm scale).

contribution is typically weak for quantum confinement, however, because of the magnitude of $(\partial E/\partial a)$.[41] Thermal expansion of the quantum-confined envelope[41] will likewise be a small effect, since the thermal expansion coefficient of Si changes sign near 100 K but is otherwise small ($\sim 10^{-6}$ K^{-1}).[43] This leaves electron−phonon coupling as the dominant factor, similar to what occurs in the bulk.[33,34,42] A rigorous expression for $E(T)$ does not exist for SiNCs, so we adopt the approach of ref 44 and fit $E(T)$ to a second order polynomial (curves, Figure 2a), where the constant term models the 0 K bandgap (E_0). Figure 2b shows the parameter E_0 fit to the expression[18,39] $E_0(R) = 1.17\ \text{eV} + 4.53/(2R)^{1.5}$ characteristic of quantum confinement, along with representative TEM images. From the fit of $E(T)$ we compute dE/dT, which we compare to bulk silicon[44] in Figure 3. The two sample types exhibit the same

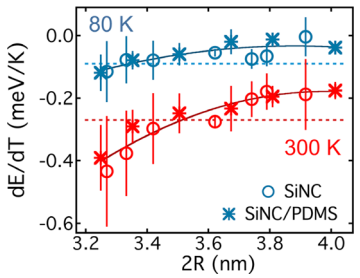

Figure 3. (a) Size dependence of dE/dT for the two sample types at 80 and 300 K, where the curves are second order polynomial fits. Bulk values from the literature are shown as dashed lines.

size-dependent deviation from bulk behavior. Assuming that larger nanocrystals would approach the bulk value of dE/dT, our data suggest that the magnitude of dE/dT should exhibit a minimum at ∼4−5 nm, which roughly coincides with the exciton Bohr radius of Si.

Despite the identical thermal behavior of the bandgap, there are some important differences between the two sample types. The PL line width is similar for the largest fractions, but the polymer nanocomposites have measurably narrower spectra at smaller nanocrystal size (Figure 4). In both cases, the full width at half-maximum (fwhm) increases weakly with decreasing temperature and decreasing size from a minimum near $2R \approx 4$ nm, with a size dependence (Figure 4c and d) that is opposite to that of dE/dT. The near-Gaussian shape of the spectra (Figure 4a) suggests that the broadening is predominantly inhomogeneous. The larger fwhm at lower T and the larger

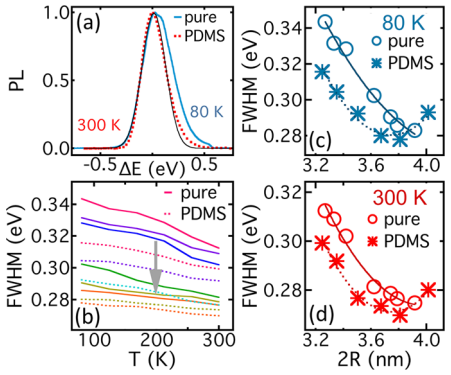

Figure 4. (a) Spectra of a fraction (f12) in PDMS at 300 K and a pure fraction (f7) at 80 K with a Gaussian profile (black). (b) PL line width (fwhm) from the measured spectra as a function of temperature for the pure SiNC fractions and the corresponding PDMS nanocomposites, where the arrow indicates the direction of increasing size. (c) fwhm for the SiNC fractions and nanocomposites as a function of size at 80 K and (d) an analogous plot at 300 K. The curves in (c) and (d) are second order polynomial fits, and the horizontal label in (c) is identical to that in (d).

fwhm in the pure SiNC films compared to the polymer nanocomposites is consistent with coupling to the "ensemble" environment that is stronger both at lower T and in pure nanocrystal films. The former effect is consistent with an increase in pressure associated with contraction upon cooling (Supporting Information), while the latter effect is consistent with a suppression of interaction effects by the polymer matrix[39] in the PDMS nanocomposites, as discussed in greater detail below.

Typical PL decay in response to pulsed UV excitation is shown in Figure 5a and b. The "stretched" nature of the background-corrected intensity, $I(t) = I_0 \exp[-(t/\tau)^{\alpha}]$, leads to noticeable curvature on a semilog plot. Figure 5c and d show lifetime maps of the two sample types in the plane of

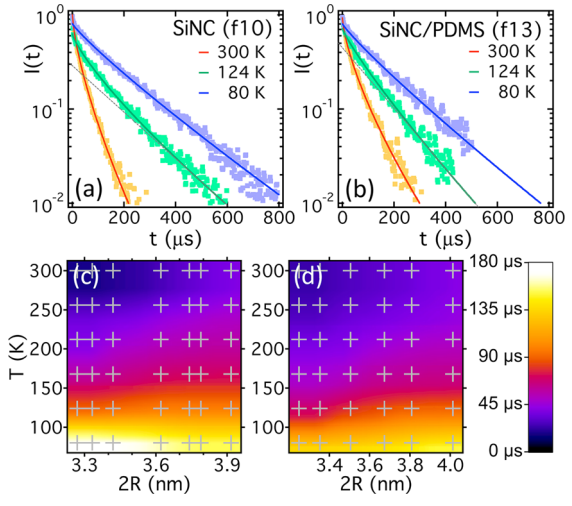

Figure 5. (a) Temporal decay of PL for a pure SiNC fraction at three different temperatures and (b) an analogous plot for a PDMS nanocomposite. The curves are the stretched-exponential fits used to extract PL lifetime, and the dashed lines highlight the deviation from purely exponential relaxation. (c) Lifetime in the plane of temperature and nanocrystal size for the pure SiNC fractions and (d) an analogous plot for the PDMS nanocomposites, where the hatch marks indicate measurement locations.

dx.doi.org/10.1021/am400411a | ACS Appl. Mater. Interfaces 2013, 5, 4233−4238

temperature and nanocrystal size, and Figure 6a suggests that the dependence of the exponent α on R and T is the same for

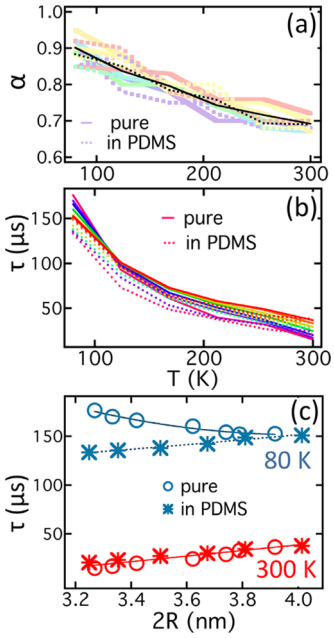

Figure 6. (a) Exponent α as a function of temperature for pure SiNCs (solid) and PDMS nanocomposites (dashed). The black trace is the fraction average. (b) Lifetime vs T for pure SiNCs (solid) and PDMS nanocomposites (dashed). The color key is the same as in Figures 1 and 2 and the label for the horizontal axis in (a) is the same as that for (b). (c) Lifetime as a function of nanocrystal size for pure SiNCs and PDMS composites at 300 and 80 K. Error bars are the size of the markers.

the two sample types. Stretched-exponential relaxation typically arises from a broad superposition of exponential decays, where for nanocrystalline silicon this distribution can reflect phonons, surface trap states, or recombination centers.[43,45−50] It has recently been suggested that multiexponential relaxation is in fact intrinsic to indirect bandgap semiconductor nanocrystals.[49] In light of the monodisperse nature of the fractions and the insensitivity of α to sample type, the data presented here support an intrinsic origin, with the $\alpha \rightarrow 1$ trend at low T reflecting a decrease in the number of available phonon modes upon cooling. Figure 6b shows how τ evolves with T, and Figure 6c shows the trends with size at low and high temperature. Although otherwise similar, an increase in τ with decreasing R is clearly evident for the pure SiNC films at 80 K Figure 6c).

A handful of recent studies have focused on the PL of size-purified SiNCs,[39,51−53] and an increase in lifetime with increasing nanocrystal size can be anticipated up to the characteristic size corresponding to the optimum quantum yield. A striking exception to this trend is the low temperature behavior exhibited by the pure SiNCs, which show an increase in lifetime with decreasing size. A hint of this trend can also be seen in recent cryogenic measurements on size polydisperse solution-synthesized SiNCs,[37] although only two nanocrystal sizes were examined in that study. In the simplest view, the quantum yield is $\Phi = k_0/(k_0 + k')$, where k_0 and k' are equilibrium constants associated with radiative and nonradiative relaxation, respectively. The lifetime is $\tau = (k_0 + k')^{-1}$ and the radiative $(T \rightarrow 0)$ lifetime is $\tau_0 = (k_0)^{-1}$, with $\tau_{\mathrm{Pure}}/\tau_{\mathrm{PDMS}} = (k_0 + k')_{\mathrm{PDMS}}/(k_0 + k')_{\mathrm{Pure}}$. The assumption that k_0 is intrinsic to an individual nanocrystal implies

$$\frac{\tau_{\mathrm{Pure}}}{\tau_{\mathrm{PDMS}}} = \frac{\Phi_{\mathrm{Pure}}}{\Phi_{\mathrm{PDMS}}} = \frac{1 + (k'/k_0)_{\mathrm{PDMS}}}{1 + (k'/k_0)_{\mathrm{Pure}}} \quad (1)$$

with the behavior in Figure 6c thus suggesting that there is a low-temperature decrease in the nonradiative rate constant $(k')_{\mathrm{Pure}}$ with decreasing size. For both sample types, a decrease in k' upon cooling leads to an increase in τ, but our data suggest that the low-T decrease in k' is more pronounced for the pure SiNC films at smaller nanocrystal diameters.

A feasible explanation for this difference is the influence of interactions, which appear to reduce nonradiative rates in SiNC clusters.[39] We note that a somewhat related but different trend has recently been predicted by many-body theory, where room-temperature exciton transport rates and PL relaxation rates both increase with decreasing nanoparticle separation and decreasing nanocrystal size.[38] Such computational schemes are better suited to smaller SiNCs,[38] however, and are inconclusive at the close separations of interest here. They also use local field factors to approximate the screening of interdot Coulomb interactions and neglect any role for "dark" trap states. Here, insight into the origin of the effect comes from its notable absence in the PDMS nanocomposites. A previous study of PL enhancement in size-purified SiNCs showed a correlation between PL and ensemble microstructure; clusters slowly dried from neat SiNC solutions showed PL "brightening", while clusters formed quickly in composite films through phase separation in polymer solutions showed "bleaching".[39] The important differences are the tendency for packing order in the pure SiNC films[39] (whereas the SiNC clusters in the polymer nanocomposites are amorphous) and the presence of residual interfacial polymer in the nanocomposite clusters. Although more research is clearly warranted, both of these have the potential to influence the collective optical response through interactions, particularly at low temperature. Here, the PDMS nanocomposites also show significant phase separation between the nanocrystals and the polymer matrix (Supporting Information), suggesting that the same morphological factors that influence room-temperature PL "brightening" might also influence the low-temperature PL relaxation behavior reported here.

Finally, we utilize the above observations to fabricate the first PL-based fiber-optic cryothermometer from SiNCs. A typical device is shown in Figure 7 and details of the fabrication scheme are given in the Supporting Information. The device relies on the transmission of excitation light through one fiber and the collection of PL through another (parallel) fiber, with the SiNCs assembled as a film on the common end (Figure 7a). The labeled end is then placed inside a cryostage while the temperature is changed. The PL response from these prototype devices is sufficient to provide an optical metric of temperature with a potentially small footprint (~ 1 mm), which might open up routes to new cryo-sensing and thermometry applications. Interestingly, devices fabricated from the PDMS nanocomposites had stronger signal than devices fabricated from the pure SiNCs, suggesting that despite the above differences in quantum yield, the polymer nanocomposites are better for making devices. Optical inspection of the labeled ends of the fibers revealed a more uniform coverage for the PDMS nanocomposites, highlighting one of the major advantages of polymer coating technology.

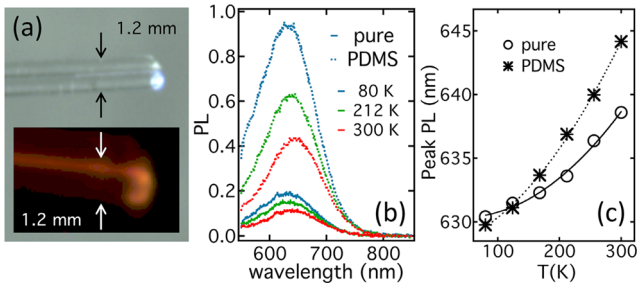

Figure 7. (a) Normal and PL (inset) color images of a fiber-optic cryothermometer made from a middle SiNC fraction in PDMS. The excitation is introduced through the bottom fiber and PL is collected through the top. (b) Emission spectra as a function of temperature for fiber-optic devices made from both pure SiNCs and a PDMS nanocomposite. (c) Wavelength of peak PL as a function of temperature for the two devices shown in (b).

CONCLUSIONS

We have characterized the temperature dependent PL of highly monodisperse size-purified SiNCs in pure nanocrystal films and PDMS nanocomposites from room temperature down to 80 K. We find behavior consistent with weaker interparticle/environmental coupling in the PDMS nanocomposites and stronger interparticle effects in the pure SiNC films, but the overall behavior is in agreement with the trends that would be expected based on the thermal behavior of bulk silicon and the influence of quantum confinement. The line width is slightly larger at low temperature (consistent with stronger coupling to the local environment at lower T) and somewhat smaller in the nanocomposites (consistent with weaker ensemble coupling due to the cross-linked polymer matrix). The functional form of the PL decay is a stretched-exponential relaxation independent of sample type (pure vs nanocomposite), consistent with coupling to a distribution of internal phonon modes.

The lifetime for both samples increases with decreasing temperature, but an unanticipated low-T increase in τ with decreasing nanocrystal size in the pure SiNC films is suggestive of an increase in ensemble quantum yield mediated by nanocrystal interactions. A feasible explanation for the absence of this enhanced lifetime in the PDMS nanocomposites would then be the influence of intervening polymer on the interaction of neighboring nanocrystals. Although perhaps less sensitive to changes in temperature than the PL from the pure SiNC films, the intensity, lifetime, and wavelength of the PDMS nanocomposites is sufficient to provide a measure of local temperature in a polymer-dispersed morphology suitable for biomedical applications. The flexible transparent PDMS matrix also offers a convenient way to contain and protect the SiNC fluorophores, while preventing their loss into the environment and maintaining a more uniform coating on the fiber ends. Although an apparent suppression of low-temperature many-body effects by the intervening polymer matrix might reduce the ensemble quantum yield, it might also have a stabilizing influence on the PL, which could be critical for sensing applications that demand reproducibility.

MATERIALS AND METHODS

Materials. The nanoparticles were plasma synthesized and surface processed with a 5:1 mixture of mesitylene and a ligand (1-dodecene) through a liquid-phase thermal hydrosilylation reaction.[9,10,40] The SiNCs were then further purified by size using DGU as detailed elsewhere.[39,53,54] Pure and PDMS composite films of SiNC fractions were prepared on quartz or glass coverslips. For the PDMS, a 10:1 by mass ratio of monomer to hardener was used for the films and 20:1 was used for the devices. Resin and catalyst were combined in a vial and stirred for 5 min. A small amount (~100 mg) of mixed PDMS was placed in another vial and then combined with toluene to form a 2% by weight PDMS/toluene solution. This parent solution was then used for all PDMS/SiNC samples. The coverslips were UVO plasma cleaned and then annealed in perfluorodecyltriethoxysilane vapor to generate a fluorinated self-assembled monolayer (SAM), which enables control of film thickness (and total PL signal) through the rate of solvent evaporation on a partially wetting surface. Composite and pure SiNC films were drop cast from toluene or hexane, respectively, onto treated coverslips, and in the case of PDMS annealed under vacuum at 40 °C for 1 h to promote cross-linking. Polymer nanocomposites prepared in this fashion showed limited phase separation at the time of measurement (immediately after preparation), but such samples coarsened considerably over the span of days (Supporting Information).

Methods. Transmission-electron microscopy (TEM) images were taken with a JEOL JEM-2100 analytical TEM operated at 200 kV. Digital images were collected using a GATAN Orius SC1000 bottom-mount CCD. Quantifoil grids containing an orthogonal array of microscopic holes on a 200 mesh copper support were cleaned with chloroform and toluene, dried under vacuum, and then placed on a UVO plasma cleaned coverslip. A small volume (10 μL) of purified water was introduced onto the grid, followed by 20 μL of a nanocrystal fraction dispersed in toluene. The toluene quickly evaporates to leave a monolayer of nanocrystals on the water surface, and this monolayer gets suspended over the grid as the water evaporates (TEM images in Supporting Information). Optical measurements were generated using nearly simultaneous visible/NIR fluorescent imaging and visible/NIR fluorescence lifetime spectroscopy on a customized upright microscope. All PL measurements were taken in transmission mode with a 4× long-working-distance NA 0.13 objective. A collimated variable-power 1 mW fiber-coupled LED (365 nm) was used for continuous excitation, and modulated pulsed excitation was delivered with a fiber-coupled pulsed UV laser (Advanced Laser Diode Systems, PiL037, 375 nm, 30 ps pulse width, 140 mW peak power, 1 kHz to 1 MHz modulation) fiber coupled to a photomultiplier tube (Hamamatsu H10721−20). Measured excitation power at the sample with the LED was typically 30 to 60 mW/cm^2, while RMS pulsed-laser excitation power at the sample was 0.2 mW/cm^2 at 1 MHz. For the pure PDMS, spectral transmission was measured using a fiber-coupled white-light LED. All measurements were performed as a function of temperature between 80 and 300 K using a Linkham BCS196 CryoBiology stage. A TA Instruments Q2000 DSC with LNCS cooling was used to measure the T_g of the pure PDMS.

ASSOCIATED CONTENT

Supporting Information

Calorimetric (DSC) characterization of the pure PDMS, optical characterization of the pure PDMS as a function of temperature, measurements of SiNC phase separation in the PDMS nanocomposites as a function of time, details related to the fabrication of the fiber-optic devices, and typical TEM images and corresponding size distributions. This material is available free of charge via the Internet at http://pubs.acs.org.

AUTHOR INFORMATION

Corresponding Author

*E-mail: erik.hobbie@ndsu.edu.

Notes

The authors declare no competing financial interest.

ACKNOWLEDGMENTS

E.K.H. acknowledges the support of the NSF through CBET-1133135 and the DOE through DE-FG36-08GO88160. R.J.A.

and U.R.K. acknowledge primary support through the NSF under MRSEC Grant DMR-0819885.

REFERENCES

(1) Zhuang, L.; Guo, L.; Chou, S. Y. *Appl. Phys. Lett.* **1998**, *72*, 9−11.
(2) Oosterhout, S. D.; Wienk, M. M.; van Bavel, S. S.; Thiedmann, R.; Jan Anton Koster, L.; Gilot, J.; Loos, J.; Schmidt, V.; Janssen, R. A. J. *Nat. Mater.* **2009**, *8*, 818−824.
(3) Feng, M.; Silverman, K. L.; Mirin, R. P.; Cundiff, S. T. *Opt. Express* **2010**, *18*, 13385−13395.
(4) Haverinen, H. M.; Myllylä, R. A.; Jabbour, G. E. *J. Display Technol.* **2010**, *6*, 87−89.
(5) Erogbogbo, F.; Yong, K.-T.; Roy, I.; Xu, G.; Prasad, P. N.; Swihart, M. T. *ACS Nano* **2008**, *2*, 873−878.
(6) Tada, H.; Higuchi, H.; Wanatabe, T. M.; Ohuchi, N. *Cancer Res.* **2007**, *67*, 1138.
(7) Kirchner, C.; Liedl, T.; Kudera, S.; Pellegrino, T.; Javier, A. M.; Gaub, H. E.; Stölzle, S.; Fertig, N.; Parak, W. J. *Nano Lett.* **2005**, *5*, 331−338.
(8) Derfus, A. M.; Chan, W. C. W.; Bhatia, S. N. *Nano Lett.* **2004**, *4*, 11−18.
(9) Mangolini, L.; Thimsen, E.; Kortshagen, U. *Nano Lett.* **2005**, *5*, 655−659.
(10) Anthony, R. J.; Rowe, D. J.; Stein, M.; Yang, J.; Kortshagen, U. *Adv. Funct. Mater.* **2011**, *21*, 4042−4046.
(11) Pi, X. D.; Liptak, R. W.; Nowak, J. D.; Wells, N.; Carter, C. B.; Campbell, S.; Kortshagen, U. *Nanotechnology* **2008**, *19*, 245603.
(12) Fujioka, K.; Hiruoka, M.; Sato, K.; Manabe, N.; Miyasaka, R.; Hanada, S.; Hoshino, A.; Tilley, R. D.; Manome, Y.; Hirakuri, K.; Yamamoto, K. *Nanotechnology* **2008**, *19*, 415102.
(13) Ding, Z.; Quinn, B. M.; Haram, S. K.; Pell, L. E.; Korgel, B. A.; Bard, A. J. *Science* **2002**, *296*, 1293−1297.
(14) Warner, J. H.; Hoshino, A.; Yamamoto, K.; Tilley, R. D. *Angew. Chem., Int. Ed.* **2005**, *117*, 4626−4630.
(15) Park, J.-H.; Gu, L.; Maltzahn, G.; Ruoslahti, E.; Bhatia, S. N.; Sailor, M. J. *Nat. Mater.* **2009**, *8*, 331−336.
(16) Mangolini, L.; Kortshagen, U. *Adv. Mater.* **2007**, *19*, 2513−2519.
(17) Liu, C.-Y.; Holman, Z. C.; Kortshagen, U. R. *Nano Lett.* **2009**, *9*, 449−452.
(18) Ledoux, G.; Gong, J.; Huisken, F.; Guillois, O.; Reynaud, C. *Appl. Phys. Lett.* **2002**, *80*, 4834−4837.
(19) Wray, S.; Cope, M.; Delpy, D. T.; Wyatt, J. S.; Reynolds, E. O. R. *Biochim. Biophys. Acta* **1998**, *933*, 184−192.
(20) Choi, J.; Zhang, Q.; Reipa, V.; Wang, N. S.; Stratmeyer, M. E.; Hitchins, V. M.; Goering, P. L. *J. Appl. Toxicol.* **2009**, *29*, 52−60.
(21) Hannah, D. C.; Yang, J.; Podsiadlo, P.; Chan, M. K. Y.; Demortiere, A.; Gosztola, D. J.; Prakapenka, V. B.; Schatz, G. C.; Kortshagen, U. R.; Schaller, R. D. *Nano Lett.* **2012**, *12*, 4200−4205.
(22) Sykora, M.; Mangolini, L.; Schaller, R. D.; Kortshagen, U.; Jurbergs, D.; Klimov, V. I. *Phys. Rev. Lett.* **2008**, *100*, 067401.
(23) Walker, G. W.; Sundar, V. C.; Rudzinski, C. M.; Wun, A. W.; Bawendi, M. G.; Nocera, D. G. *Appl. Phys. Lett.* **2003**, *83*, 3555−3557.
(24) Walker, G. W.; Sundar, V. C.; Rudzinski, C. M.; Wun, A. W.; Bawendi, M. G.; Nocera, D. G. *Appl. Phys. Lett.* **2003**, *83*, 3555−3557.
(25) Barmenkov, Y. O.; Starodumov, A. N.; Lipovski, A. A. *Appl. Phys. Lett.* **1998**, *73*, 541−543.
(26) de Bastida, G.; Arregui, F. J.; Goicoechea, J.; Matias, I. R. *IEEE Sens. J.* **2006**, *6*, 1378−1379.
(27) Jorge, P. A. S.; Mayeh, M.; Benrashid, R.; Caldas, P.; Santos, J. L.; Farahi, F. *Meas. Sci. Technol.* **2006**, *17*, 1032−1038.
(28) Jorge, P. A. S.; Maule, C.; Silvia, A. J.; Benrashid, R.; Santos, J. L.; Farahi, F. *Anal. Chim. Acta* **2008**, *606*, 223−229.
(29) Bullen, C.; Mulvaney, P.; Sada, C.; Ferrari, M.; Chiasera, A.; Martucci, A. *J. Mater. Chem.* **2004**, *14*, 1112−1116.
(30) Yoo, J.; Park, S. J.; Kim, J. S. *Mol. Cryst. Liq. Cryst.* **2010**, *519*, 62−68.
(31) Han, B.; Hanson, W. L.; Bensalah, K.; Tuncel, A.; Stern, J. M.; Cadeddu. *Ann. Biomed. Eng.* **2009**, *37*, 1230−1239.
(32) Onik, G. M.; Atkinson, D.; Zemel, R.; Weaver, M. L. *Semin. Surg. Oncol.* **2006**, *9*, 309−317.
(33) Hartel, A. M.; Gutsch, S.; Hiller, D.; Zacharias, M. *Phys. Rev. B* **2012**, *85*, 165306.
(34) Wang, X. X.; Zhang, J. G.; Ding, L.; Cheng, B. W.; Ge, W. K.; Yu, J. Z.; Wang, Q. M. *Phys. Rev. B* **2005**, *72*, 195313.
(35) Wen, X.; Van Dao, L.; Hannaford, P. *J. Phys. D: Appl. Phys.* **2007**, *40*, 3573−578.
(36) Rinnert, H.; Jambois, O.; Vergnat, M. *J. Appl. Phys.* **2009**, *106*, 023501.
(37) Maier-Flaig, F.; Henderson, E. J.; Valouch, S.; Klinkhammer, S.; Kübel, C.; Ozin, G. A.; Lemmer, U. *Chem. Phys.* **2012**, *405*, 175−180.
(38) Lin, Z.; Li, H.; Franceschetti, A.; Lusk, M. T. *ACS Nano* **2012**, *6*, 4029−4038.
(39) Miller, J. B.; Van Sickle, A. R.; Anthony, R. J.; Kroll, D. M.; Kortshagen, U. R.; Hobbie, E. K. *ACS Nano* **2012**, *6*, 7389−7396.
(40) Kortshagen, U.; Mangolini, L.; Bapat, A. *J. Nanopart. Res.* **2007**, *9*, 39−52.
(41) Olkhovets, A.; Hsu, R.-C.; Lipovskii, A.; Wise, F. W. *Phys. Rev. Lett.* **1998**, *81*, 3539−3542.
(42) O'Donnell, K. P.; Chen, X. *Appl. Phys. Lett.* **1991**, *58*, 2924−2926.
(43) Lyon, K. G.; Salinger, G. L.; Swenson, C. A.; White, G. K. *J. Appl. Phys.* **1977**, *48*, 865−869.
(44) Bludau, W.; Onton, A.; Heinke, W. *J. Appl. Phys.* **1974**, *45*, 1846−1848.
(45) Mauckner, G.; Thonke, K.; Baier, T.; Walter, T.; Sauer, R. *J. Appl. Phys.* **1994**, *75*, 4167.
(46) Pavesi, L. *J. Appl. Phys.* **1996**, *80*, 216−226.
(47) Chen, R. *J. Lumin.* **2003**, *102*−*103*, 510−518.
(48) Heitmann, J.; Müller, F.; Yi, L.; Zacharias, M.; Kovalev, D.; Eichhorn, F. *Phys. Rev. B* **2004**, *69*, 195309.
(49) Delerue, C.; Allan, G.; Reynaud, C.; Guillois, O.; Ledoux, G.; Huisken, F. *Phys. Rev. B* **2006**, *73*, 235318.
(50) Linnros, J.; Lalic, N.; Galeckas, A.; Grivickas, V. *J. Appl. Phys.* **1999**, *86*, 6128−6134.
(51) Mastronardi, M. L.; Maier-Flaig, F.; Faulkner, D.; Henderson, E. J.; Kübel, C.; Lemmer, U.; Ozin, G. A. *Nano Lett.* **2012**, *12*, 337−342.
(52) Hessel, C. M.; Reid, D.; Panthani, M. G.; Rasch, M. R.; Goodfellow, B. W.; Wei, J.; Fujii, H.; Akhavan, V.; Korgel, B. A. *Chem. Mater.* **2012**, *23*, 393−401.
(53) Mastronardi, M. L.; Hennrich, F.; Henderson, E. J.; Maier-Flaig, F.; Blum, C.; Reichenbach, J.; Lemmer, U.; Kübel, C.; Wang, D.; Kappes, M. M.; et al. *J. Am. Chem. Soc.* **2011**, *133*, 11928−11931.
(54) Bai, L.; Ma, X.; Liu, J.; Sun, X.; Zhao, D.; Evans, D. G. *J. Am. Chem. Soc.* **2010**, *132*, 2333−2337.